Removal of trivalent metal ions from aqueous solution via cross-flow ultrafiltration system using zeolite membranes

Ashim Kumar Basumatary, R. Vinoth Kumar, Kannan Pakshirajan and G. Pugazhenthi

ABSTRACT

This study aimed to assess the performance of three zeolite membranes in the removal of trivalent metal ions from aqueous solution using a cross-flow mode of operation. Three types of zeolite membrane, MCM-41, MCM-48 and FAU, were prepared on a low-cost, circular ceramic support by hydrothermal treatment. The three zeolite membranes were characterized by using X-ray diffraction (XRD), field emission scanning electron microscopy (FESEM) and contact angle measurements. The XRD results confirmed the formation of zeolites. The deposition of zeolite on the ceramic support and hydrophilicity of zeolite membranes were monitored by FESEM and contact angle measurement, respectively. The pore size of the MCM-41, MCM-48 and FAU membrane was found to be 0.173 μm, 0.142 μm, and 0.153 μm, respectively, which was lower than that of the support (1.0 μm). The fabricated zeolite membranes were used to investigate the separation behavior of trivalent metal ions (Al^{3+} and Fe^{3+}) from aqueous solution at various applied pressures. It was observed that an increase of applied pressure leads to a slight decrease in the removal efficiency. Among the various zeolite membranes, the FAU membrane showed the maximum rejection of 88% and 83% for Fe^{3+} and Al^{3+} separation, respectively.

Key words | membrane separations, pollutants, separation, water treatment, zeolites

Ashim Kumar Basumatary
R. Vinoth Kumar
G. Pugazhenthi (corresponding author)
Department of Chemical Engineering,
Indian Institute of Technology Guwahati,
Guwahati 781039,
Assam,
India
E-mail: *pugal@iitg.ernet.in*

Kannan Pakshirajan
Department of Biosciences and Bioengineering,
Indian Institute of Technology Guwahati,
Guwahati 781039,
Assam,
India

INTRODUCTION

Metal ions in wastewater are a serious environmental concern owing to their high toxicity and tendency to accumulate in living organisms (Mohammad *et al.* 2004). These metals are non-biodegradable in the environment; therefore, environmental regulations are designed to reduce the level of concentration in wastewater to the safe limit specified by legislation. Sources of contamination in wastewater include printing, tanning, electroplating, dying and textile industries, steel working and finishing industries, battery manufacturing units, chlorinating agents in metallurgical and organic synthesis, and catalysts (Gherasim *et al.* 2013). When wastewater from various industrial activities is discharged into the environment, the standards of environmental regulations should be implemented. Therefore, the treatment of wastewater for the removal of contaminants becomes an important and challenging task.

Conventional techniques for the removal of effluent coming from various sources of streams are liquid–liquid extraction, precipitation, adsorption and ion exchange (Kumar *et al.* 2015a, 2015b). These methods are time consuming, laborious, expensive and cannot reduce the pollutants to the limit framed by legislation. In addition, reverse osmosis, electrodialysis, and nanofiltration have been used for wastewater treatment (Gherasim *et al.* 2013). However, these processes are expensive and have limitations due to high pressure requirements. Therefore, it is necessary to explore an alternative, cheaper, efficient and non-polluting separation technique. Charged ultrafiltration membranes are gaining popularity in wastewater treatment due to their

doi: 10.2166/wrd.2016.211

capability for electrostatic interactions between a charged membrane and metal ions, even when wide pore membranes are used (Arunkumar & Etzel 2015).

Membrane technologies are promising methods for the separation of heavy metals from aqueous solutions (Frares *et al.* 2005). Moreover, membrane-based separations are more effective in terms of energy saving, higher removal efficiency and stability in operation. Conversely, organic polymeric membranes showed instability at high temperature and in harsh environments. Over the past two decades, supported inorganic zeolite membranes have been utilized in various applications such as separators, sensors, reactors and electrical insulators because of their uniform pore structure framework and high thermal stability (Yu *et al.* 2007; Ahmad & Hagg 2013). Sandstrom *et al.* (2011) prepared an MFI zeolite membrane on an alumina support to separate CO_2 gas from synthesis gas and natural gas. Wirawan *et al.* (2011) fabricated a silicate-1 composite membrane on an α-alumina support and studied H_2/CO_2 permeation through the membrane. Maghsoudi & Soltanieh (2014) developed a CHA zeolite membrane on α-alumina disks by *in situ* crystallization to separate CO_2 and H_2S from CH_4. Iglesia *et al.* (2006) synthesized an MCM-48 membrane on an α-alumina tube and used it for the separation of gas mixtures. In addition, it is well known that the separation of metal ions by ultrafiltration and microfiltration is not only based on the pore size, but also depends on other factors such as the surface charge of the membrane and electrostatic interactions between the membrane and charged ions (Monash *et al.* 2010). This means that the interaction between membrane and metal ions can significantly affect the performance of the ultrafiltration/microfiltration membranes (Monash *et al.* 2010). Zeolites have potential for use in removing diverse materials because of their properties, including high surface area, excellent thermal/hydrothermal stability, high shape-selectivity and superior ion-exchange ability, which form the basis for their traditional applications in catalysis and separation of small molecules (Ozin *et al.* 1989; Kumar *et al.* 2015a, 2015b).

Many researchers have used α-alumina as a support material to fabricate zeolite membranes. From an industrial point of view, alumina is a very expensive material. Moreover, the majority of researchers have utilized these fabricated zeolite membranes for gas phase separation applications. The present work focuses on the preparation of MCM-41, MCM-48 and FAU (faujasite) zeolite membranes on low-cost support material and their performance in the separation of Al^{3+} and Fe^{3+} from aqueous solution.

MATERIALS AND METHODS

Materials

The raw materials used for the preparation of ceramic supports (quartz, feldspar, ball clay, pyrophyllite and kaolin) were acquired from Kanpur, India. Calcium carbonate, polyvinyl alcohol (PVA), tetraethyl orthosilicate (TEOS), aluminum fine powder and hydrochloric acid were purchased from Merck (I), Mumbai, India. Fumed silica (Aerosil 200) was procured from CDH, Laboratory Reagents, Mumbai. Ferric chloride, aluminum chloride (hexahydrate), and NaOH were bought from Loba Chemie (Laboratory Reagents & Fine Chemicals), Mumbai. All chemicals and reagents were used directly without further purification. Water was taken from the Millipore water system (ELIX-3).

Preparation of zeolite membranes

Ceramic supports were fabricated using inexpensive clay materials available in India. Details of the composition of raw materials and preparation procedure were reported in our earlier publication (Monash & Pugazhenthi 2011). Ball clay (17.58 g), pyrophyllite (14.73 g), quartz (26.59 g), kaolin (14.45 g), feldspar (5.60 g) and calcium carbonate (17.14 g) were mixed with 4 ml of 2 wt% of aqueous PVA in a ball mill. An estimated quantity of powder mixture was pressed at 50 MPa in a hydraulic press and the raw ceramic supports were sintered at 950 °C in a muffle furnace. The sintered ceramic supports were polished with abrasive paper (no. C-220) and the loose particles produced while sizing were removed in an ultrasonic bath with Millipore water for 15 min. Finally, the dried ceramic supports were subjected to hydrothermal treatment to deposit the MCM-41, MCM-48 and FAU zeolites individually on the surfaces. The cost of the ceramic support was evaluated to be Rs. 480/m^2 ($10/$m^2$) based on the cost of raw materials (Monash & Pugazhenthi 2011).

The MCM-41 zeolite membrane was synthesized with the molar composition of 1TEOS:0.1CTAB:0.3NaOH:60H_2O according to the procedure described in our previous publication

(Basumatary *et al.* 2015). The synthesized gel was subjected to hydrothermal reaction by placing a ceramic support in the bottom of a Teflon container autoclave reactor at 110 °C for 96 h. The MCM-48 zeolite membrane was fabricated with a gel composition of 1TEOS:0.25Na_2O:0.65CTAB:0.62H_2O and subjected to hydrothermal treatment at 110 °C for 72 h. After treatment, the membranes and zeolite powders (MCM-41 and MCM-48) were washed with Millipore water and dried at 100 °C for 24 h. The membranes and zeolite powders were calcined at 550 °C for 5 h for MCM-41 and 6 h for MCM-48 at a heating rate of 1 °C/min. MCM-41 and MCM-48 deposition on the ceramic support were done with three cycles of coating in the same manner. After the third cycle, no significant weight increment was observed for MCM-41 and MCM-48 membranes.

The FAU zeolite membrane was fabricated with a gel mixture of 70Na_2O:Al_2O_3:20SiO_2:2000H_2O. The prepared solution mixture and ceramic support were kept in the bottom of the autoclave reactor and treated hydrothermally at 75 °C for 24 h. After completion of the reaction, the membrane and FAU powder were washed with Millipore water and dried at 110 °C for 24 h.

Characterization

The phase purity and crystallinity of the MCM-41, MCM-48 and FAU zeolite powders were confirmed by X-ray diffraction (XRD) analysis. The XRD profile was recorded on a Bruker D8 Advance using CuKα ($\lambda = 1.5406$ A°) radiation operating at 40 kV and 40 mA. The XRD patterns were taken in the 2θ range of 1–10 ° for the MCM-41 and MCM-48 powder and 1–50 ° for the FAU powder at a scanning speed of 0.02 °s^{-1}. The structural morphology of the ceramic support and zeolite membranes were investigated by a field emission scanning electron microscope (FESEM) using a Zeiss Sigma instrument at 3-Kev acceleration voltage. Prior to FESEM analysis, the surface of the samples was coated with gold by means of a JEOL JFC-1300 auto fine coater. The wettability surface nature of the ceramic support and zeolite membranes (MCM-41, MCM-48 and FAU) were measured using a contact angle Drop Shape Analyzer-DSA 25 (Kruss), maintaining a fixed water droplet size of 4 μL and a falling rate of 0.16 mL/min. Five measurements were taken at different positions of membrane surfaces and the average value was reported.

Pure water flux

A schematic of the cross-flow ultrafiltration setup is shown in Figure 1. The cross-flow setup consists of a feed tank, pressure gauge, assembled membrane module, high pressure peristaltic pump, rotameter (1–12 l/h) and a retentate valve (needle valve). The membrane was fixed in the membrane

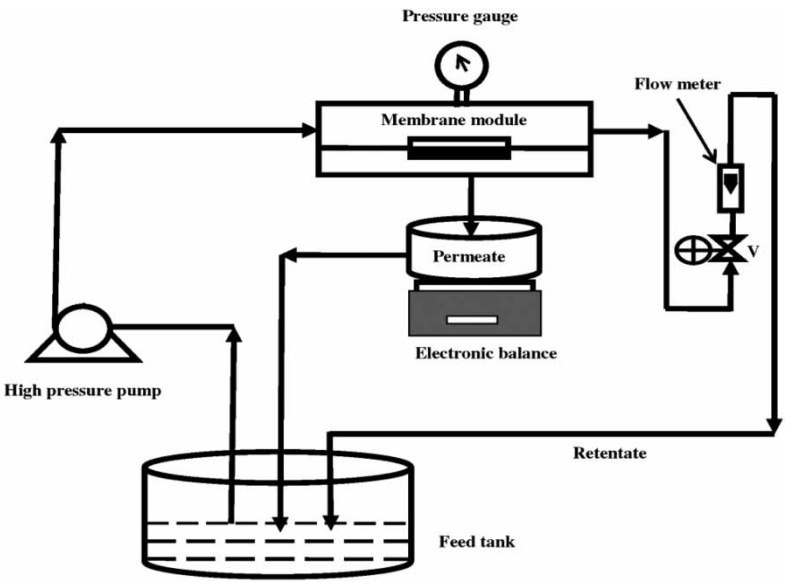

Figure 1 | Schematic of cross-flow ultrafiltration setup (V = retentate valve).

module with a perforated casing. The pure water flux of the MCM-41, MCM-48 and FAU zeolite membranes was measured at different applied pressures (69–345 kPa) at a fixed cross-flow rate of 1.667×10^{-7} m^3/s for 1 h. All experiments were performed at room temperature (~25 °C).

Cross-flow ultrafiltration of trivalent metal ions

Cross-flow filtration experiments were performed using the same setup depicted in Figure 1. Trivalent metal salts (Al^{3+} and Fe^{3+}) solutions were prepared individually with a concentration of 250 ppm using Millipore water and pH 2. A typical cross-flow ultrafiltration run involves the measurement of permeate flux at time intervals of 5 min for the separation of trivalent metal ions from aqueous solution for the time period of 1 h. With the fixed cross-flow rate (1.11×10^{-7} m^3s^{-1}), all experiments were conducted at different applied pressures (69–345 kPa) to evaluate the effect of applied pressure on the separation characteristics of all zeolite membranes. The feed solution was pumped from the feed tank container into the membrane module by means of a high pressure peristaltic pump. To examine the influence of applied pressure, the cross-flow rate was made constant by controlling the retentate valve (V) and the applied pressure was varied by adjusting the speed of the pump. In order to maintain constant concentration in the feed tank throughout the experiments, the retentate and permeate streams were returned back to the feed tank.

The concentration of feed and permeate were measured for each cross-flow ultrafiltration experiment using a conductivity meter (Eutech Instruments, Model: CON 2700). For each experimental run, the zeolite membrane was thoroughly cleaned with Millipore water followed by flushing with water at a high pressure to regain the original water flux of the membrane. The permeate flux (J) and percent rejection (R) for the separation of trivalent metal ions was determined as follows:

$$J = \frac{V}{A \times \Delta t} \tag{1}$$

$$R = 1 - \frac{C_p}{C_f} \times 100 \tag{2}$$

where V is the volume of permeate (m^3), A is the effective area of the membrane (m^2), Δt is the sampling time (s), C_f and C_p are the concentration of trivalent metal ions in the feed and permeate (ppm), respectively.

RESULTS AND DISCUSSION

Characterization

The XRD patterns of MCM-41 zeolite are shown in Figure 2(a), which illustrates the strong peak (1 0 0) and three orders of reflection (1 0 0), (1 1 0) and (2 1 0) at 2θ value of $<10^\circ$. The presence of (1 0 0), (1 1 0) and (2 0 0) diffraction peaks in the MCM-41 powder is confirmation of good crystallinity of the synthesized sample. It indicates the existence of well-resolved hexagonally arranged pore geometry as well as the high structural ordering of MCM-41. The observed XRD prototype of MCM-41 matches well with JCPD files no. 00-049-1711 for the after-calcination sample and file no. 00-049-1712 for the before-calcination sample. The XRD profile of MCM-48 (before and after calcination) is shown in Figure 2(b). The position of the 2θ value with two sharp diffraction peaks at 2.76 and 3.15 through corresponding planes of (2 1 1) and (2 2 0) illustrates the presence of the mesoporous phase of the cubical structure of MCM-48. The intensity of the peak increases after calcination when compared to the as-synthesized sample (before calcination). Hence, the ordering degree of intensity is improved due to removal of the surfactant. Similar patterns and diffractograms were also reported for MCM-48 by Wu *et al.* (2008) and Liu *et al.* (2007). Figure 2(c) displays the XRD pattern of as-synthesized FAU zeolite powder; a similar profile was reported by Huang *et al.* (2012). The peak at a 2θ value of 12.4 specified the formation of a high degree of crystallinity of FAU zeolite.

The surface morphology of the ceramic support and zeolite membranes (MCM-41, MCM-48 and FAU) are shown in Figure 3(a)–3(d). The FESEM imaging technique is employed to check the deposition and distribution of MCM-41, MCM-48 and FAU zeolites on the ceramic support. The surface morphology varies with change in the composition of precursors used for the synthesis of zeolite. The zeolite particles are uniformly distributed on the porous ceramic support, and the pores of the zeolite membranes are blocked to some extent when compared to the ceramic support as

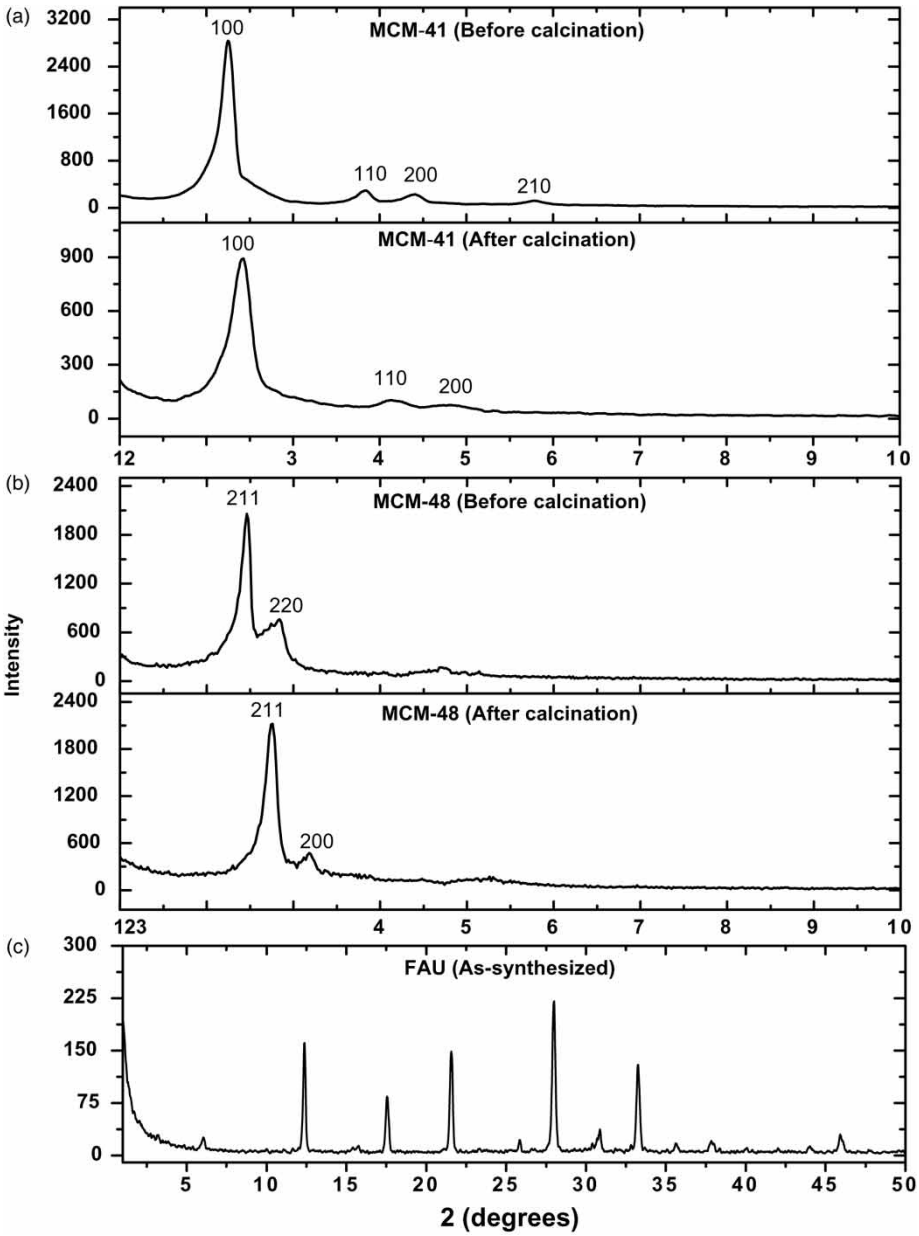

Figure 2 | XRD patterns of (a) MCM-41 (before and after calcination), (b) MCM-48 (before and after calcination), and (c) FAU zeolite (as-synthesized) powder samples.

shown in Figure 3, and principally, the formation of the cubical FAU membrane shown in Figure 3(d).

The contact angles for MCM-41, MCM-48 and FAU zeolite membranes are 38°, 28.9° and 8.4°, respectively, illustrating that the FAU membrane is more hydrophilic (Figure 4(b)–4(d)). The ceramic support has a contact angle of 81.8° (Figure 4(a)); this higher value implies that the ceramic support is more hydrophobic than the zeolite membranes. The hydrophilicity of membranes can be arranged according to their contact angle order: FAU > MCM-48 > MCM-41> ceramic support. More hydrophilic membrane surfaces leads to a reduced likelihood of fouling and concentration polarization, resulting in enhanced permeability of the solvent in the separation process.

The porosity of MCM-41, MCM-48, FAU zeolite and the ceramic support are estimated to be 23, 21, 33 and 47%,

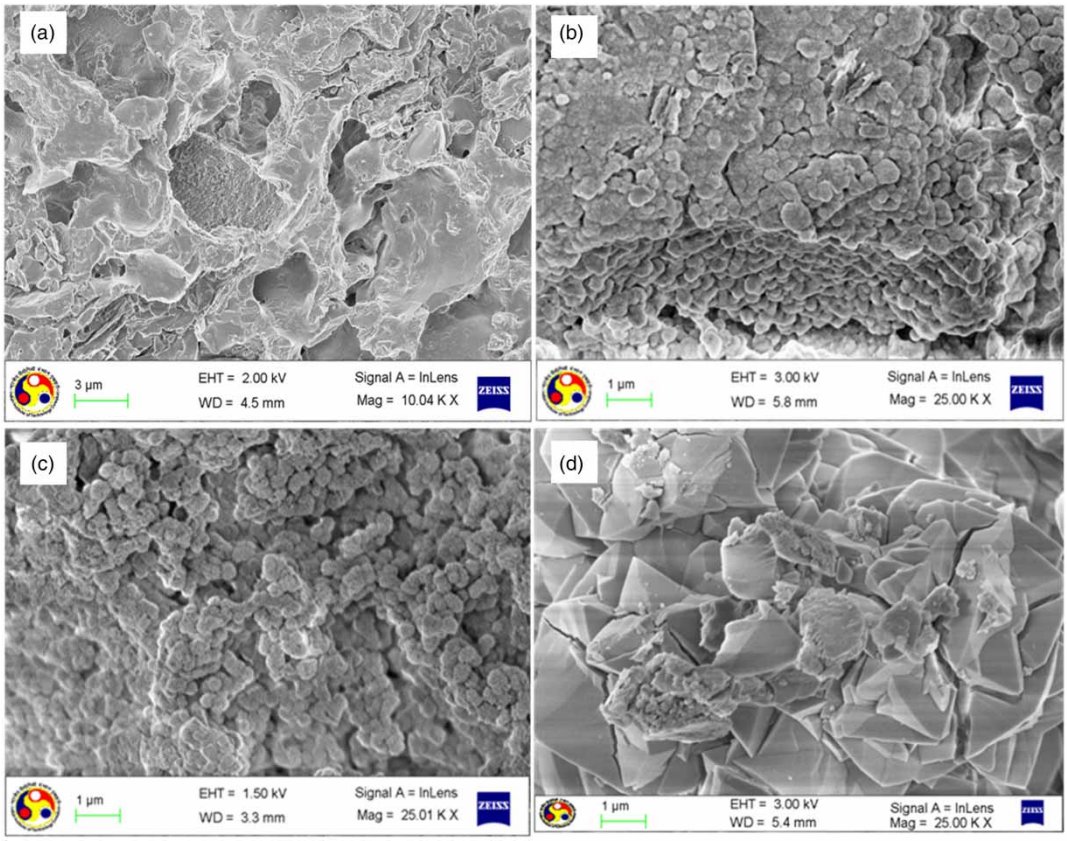

Figure 3 | FESEM images of (a) ceramic support, (b) MCM-41, (c) MCM-48 and (d) FAU zeolite membranes.

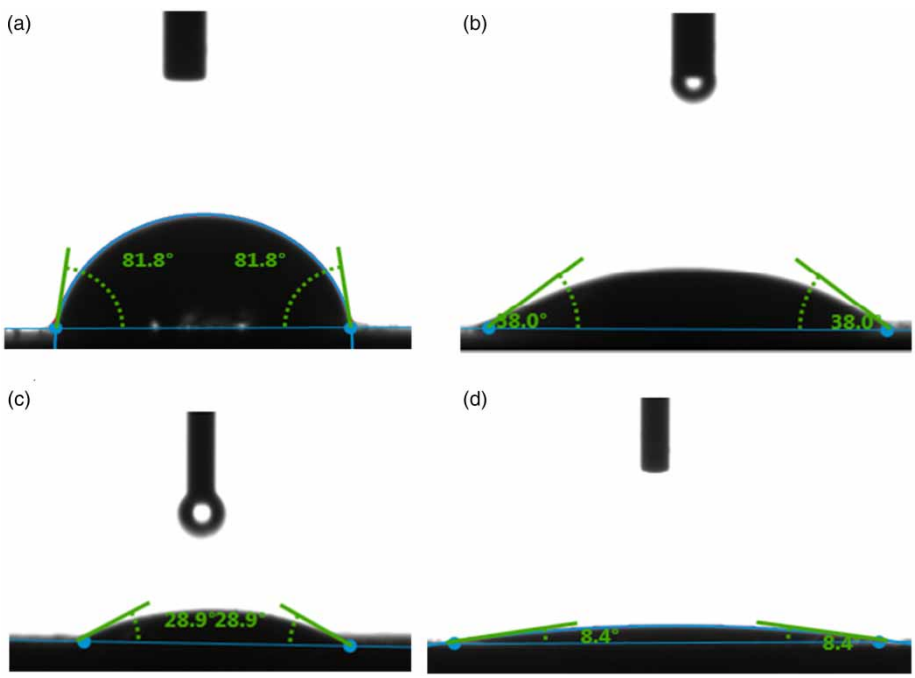

Figure 4 | Contact angles of (a) support, (b) MCM-41, (c) MCM-48 and (d) FAU zeolite membranes.

respectively, according to the method reported by Monash & Pugazhenthi (2011). It can be concluded that the deposition of zeolite materials on the ceramic support affords a reduction of porosity in the zeolite membranes. The water flux across the ceramic support and MCM-41, MCM-48 and FAU zeolite membranes is shown in Figure 5. As applied pressure increases, the pure water flux increases linearly and follows Darcy's law for all zeolite membranes. However, with the deposition of MCM-41, MCM-48 and FAU zeolite on the ceramic support, the pure water flux is drastically reduced for all zeolite membranes. The water permeability and mean pore size of the membranes are computed using the Hagen–Poiseuille equation with the batch filtration experimental setup (Kumar *et al.* 2015a, 2015b):

$$J = \frac{\varepsilon r^2 \Delta P}{8\mu\tau l} = L_h \Delta P \tag{3}$$

where J is the permeate flux (μm/s), L_h is water permeability (μm/s kPa), ΔP is the applied pressure across the membrane (kPa), μ is the viscosity of water (kPa s), l is pore length (μm), ε is the porosity of the membrane, and τ is tortuosity factor. The hydraulic permeability (L_h) is determined from the slope of the pure water flux (J) versus applied pressure across the membrane (ΔP). The water permeability (L_h) of the ceramic support, MCM-41, MCM-48 and FAU zeolite membrane was calculated as 3.63×10^{-6} m^3/m^{2}s kPa, 6.05×10^{-8} m^3/m^{2}s kPa, 4.18×10^{-8} m^3/m^{2}s kPa and 6.09×10^{-8} m^3/m^{2}s kPa, respectively. The water permeability of the prepared zeolite membranes is 2–3 orders higher than that of other membranes reported in the literature (Shukla & Kumar 2007; Workneh & Shukla 2008). The calculated average pore sizes from pure water flux are found to be 1.0 μm, 0.173 μm, 0.142 μm and 0.153 μm for the ceramic support, MCM-41, MCM-48 and FAU zeolite membranes, respectively. As stated above, the porosity, water permeability, and mean pore size of the zeolite membranes decreased, which is due to the incorporation of the zeolite layer on the ceramic support by hydrothermal treatment.

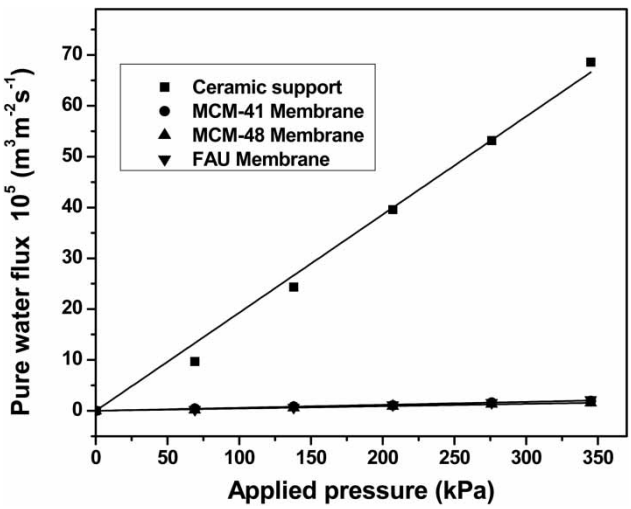

Figure 5 | Pure water flux as a function of applied pressure for support and zeolite membranes.

Separation of trivalent metal ions using cross-flow ultrafiltration

To investigate the influence of applied pressure on cross-flow ultrafiltration, the feed concentration and pH are maintained as 250 ppm and 2, respectively. The effect of permeate flux with time for MCM-41, MCM-48 and FAU zeolite membranes at different applied pressures from 69 to 345 kPa and a fixed cross-flow rate of 1.11×10^{-7} m^{3}s^{-1} is shown in Figure 6(a)–6(c). The flux of zeolite membranes increases with an increase in the applied pressure due to enhancement of the driving force. The variation of permeate flux with time is almost negligible for the entire 1 h operation as shown in Figure 6(a) for the separation of both trivalent metal ions (Al^{3+} and Fe^{3+}). Similar trends are also observed with MCM-48 and FAU zeolite composite membranes (Figure 6(b) and 6(c)) for Al^{3+} and Fe^{3+} separation. The permeate flux of all zeolite membranes varies almost linearly with increasing applied pressure. This may be explained by there being no adsorption and no significant contribution of additional transport resistance due to concentration polarization. On the other hand, the permeate flux of all zeolite membranes is slightly lower than the pure water flux of the corresponding membranes. This is due to the osmotic pressure produced by retained ions, which results in a reduction of the effective pressure across the membrane (Al-Rashdi *et al.* 2013). The permeate flux of Al^{3+} and Fe^{3+} demonstrates a similar pattern with an increase in the applied pressure for all zeolite membranes (MCM-41, MCM-48 and FAU).

The variation of the percentage rejection of Al^{3+} and Fe^{3+} using MCM-41, MCM-48 and FAU zeolite membranes

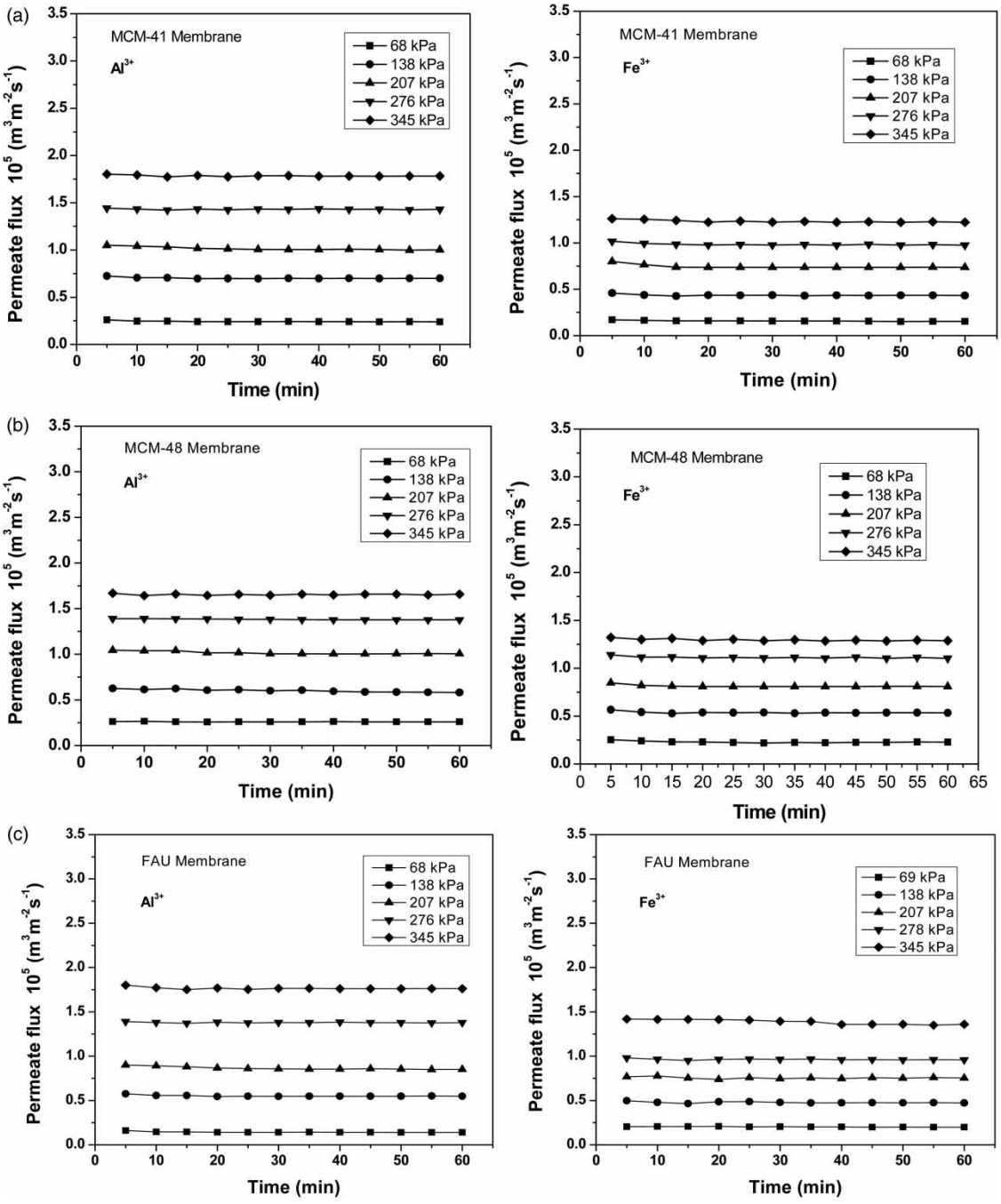

Figure 6 | Variation of permeate flux of Al^{3+} and Fe^{3+} with time at different applied pressures for (a) MCM-41, (b) MCM-48 and (c) FAU membranes (feed concentration = 250 ppm, pH = 2).

with time at different applied pressures for a fixed cross-flow rate of 1.11×10^{-7} $m^3 s^{-1}$ is presented in Figure 7(a)–7(c). For all the zeolite membranes, the rejection of trivalent metal ions slightly increases with the duration of the process. This is possibly due to a build up of the concentration polarization until a steady state is reached at the membrane surface (Danis & Keskinler 2009). The rejection also increases with increasing applied pressure for all the zeolite membranes. The convective transport becomes more important than the diffusive transport at elevated applied pressure, and hence the retention will increase. Thus, the rejection of trivalent metal ions increases with

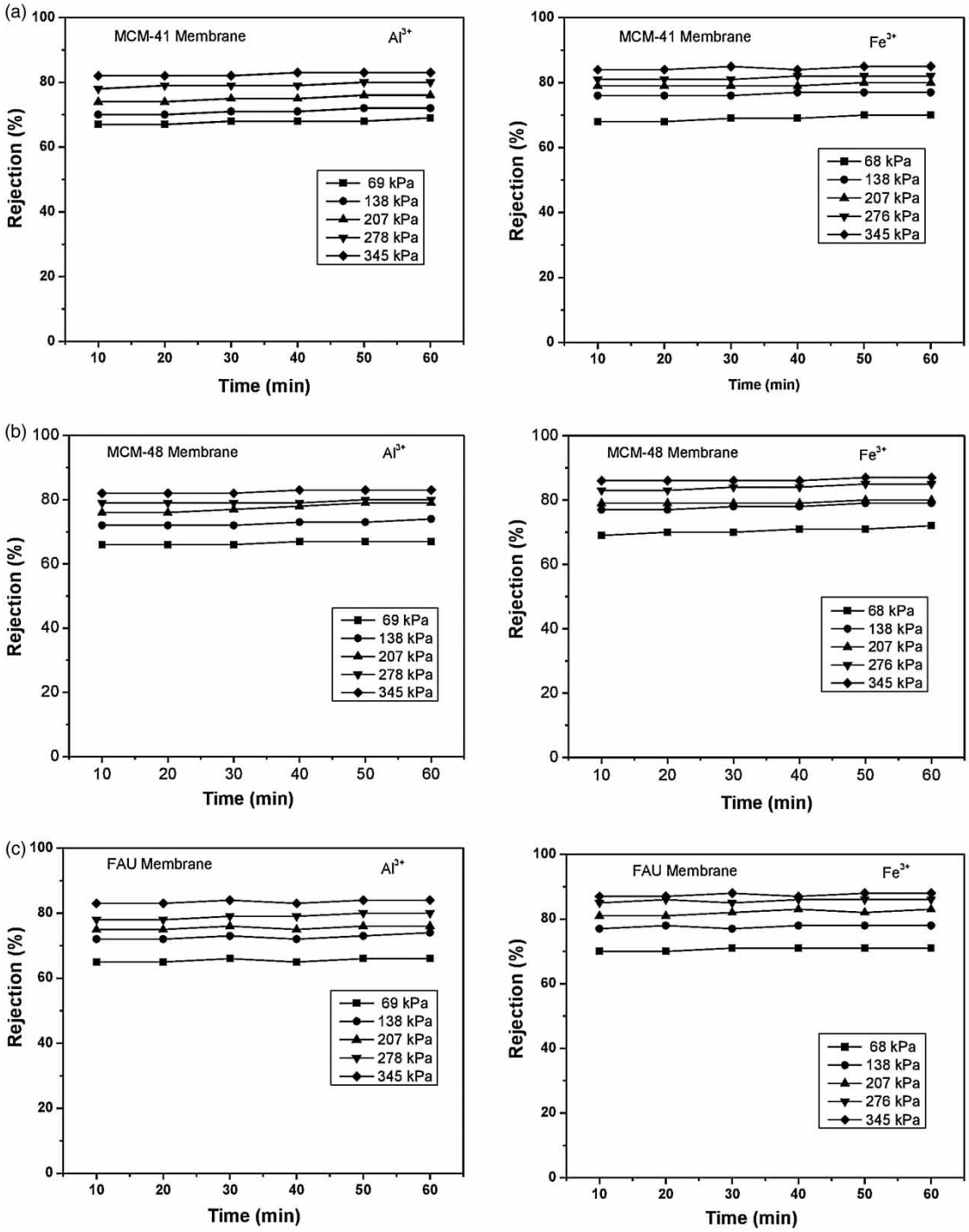

Figure 7 | Variation of rejection of Al^{3+} and Fe^{3+} with time at different applied pressures for (a) MCM-41, (b) MCM-48 and (c) FAU membranes (feed concentration = 250 ppm, pH = 2).

increasing pressure due to the dilution effect, as the higher transport solvent flux would result in a dilution of permeate. Therefore, the maximum rejection is obtained at elevated pressure (Al-Rashdi *et al.* 2013).

The surface charge of the membrane plays a significant role in determining the rejection efficiency of the membrane with ionic solution, and it differs with pH of the solution. When a charged membrane is in contact with the salt

solution, the concentration of co-ions (ions with the same charge as the membrane) close to the surface of the membrane will be lower than that in solution, and the counter-ions (having the opposite charge) have a higher concentration in the membrane than in the solution. On account of this concentration difference, a potential difference is generated at the interface between the membrane and the solution to maintain electrochemical equilibrium. By this potential (known as the Donnan potential), co-ions are repelled by the membrane (Majhi *et al.* 2009). We found the isoelectric point of the MCM-41, MCM-48 and FAU zeolite membranes to be 3.9, 3.2 and 3.8, which was determined using zeta potential measurement (Delsa Nano) (Wu *et al.* 2008). The zeta potential value of MCM-41, MCM-48 and FAU zeolite membrane is +18.36 mV, +3.95 mV and +4.22 mV, respectively, at pH 2. Since the membranes are positively charged, Al^{3+} and Fe^{3+} ions are repelled by the membrane. As cations and anions cannot act independently, Cl^{-} ions are also rejected to maintain electroneutrality. Additionally, the diffusion coefficient of Al^{3+} and Fe^{3+} also affects the retention behavior of metal ions (Schaep *et al.* 1998). Al^{3+} (5.5×10^{-9} m^2s^{-1}) has a higher diffusion coefficient than Fe^{3+} (1.4×10^{-9} m^2s^{-1}), which results in a lower rejection of Al^{3+} for all zeolite membranes (Jafarian *et al.* 2006; Haarberg & Keppert 2008). Peeters *et al.* (1998) pointed out that salts having a lower diffusion coefficient display higher retention.

In addition to charge density, the retention of trivalent metal ions also depends on the quantity of zeolite materials deposited on the ceramic support. The amount of FAU zeolite deposition (1.26 g) on the ceramic support is more than that of MCM-41 (0.89 g), whereas the zeta potential value of MCM-41 is higher than the FAU zeolite, and both membranes have very similar isoelectric point values However, the rejection of the FAU zeolite composite membrane is found to be higher when compared to the MCM-41 membrane, and this may be due to the more hydrophilic nature of the FAU zeolite membrane. Among the three zeolite membranes, the rejection of the FAU membrane is marginally higher as it has almost an equal amount of deposition to MCM-48 and its hydrophilicity is also greater than that of the other two composite membranes. The highest rejection values of 88, 86 and 85% were accomplished with the FAU, MCM-48 and MCM-41 zeolite composite membranes, respectively, at an applied pressure of 345 kPa for the removal of Fe^{3+}. In the case of Al^{3+} retention, 84, 83 and 82% were achieved using FAU, MCM-48 and MCM-41 zeolite membranes at an applied pressure of 345 kPa.

The permeate flux of trivalent metal ions showed no declining trend (i.e. no fouling of the membrane) for the MCM-41, MCM-48 and FAU zeolite membranes. In a batch filtration, there is an occurrence of concentration polarization, implying the cross-flow mode of filtration is better than the batch mode. Among the membranes in this study, the FAU zeolite membrane was found to be better in terms of flux and removal efficiency. Besides, its preparation needs less synthesis time (24 h), a lower hydrothermal temperature (75 °C), a single stage of coating and no calcination step, which leads to a lower manufacturing cost.

CONCLUSIONS

Al^{3+} and Fe^{3+} can be effectively removed using zeolite membranes (MCM-41, MCM-48 and FAU) by a cross-flow ultrafiltration mode. MCM-41, MCM-48 and FAU zeolite composite membranes do not have a tendency for fouling and cake layer formation on the surface of the membrane in the removal of trivalent metal ions. The FAU zeolite membrane displays a slightly higher rejection when compared to the other membranes and is better than MCM-41 and MCM-48 zeolite membranes due to the shorter synthesis time, single cycle deposition and having no calcination step required in its preparation. The maximum rejection is observed with Fe^{3+} separation rather than Al^{3+} for all the zeolite membranes. In the experiment, a permeate flux decline trend was not observed during the whole period of the filtration study; hence the prepared zeolite membranes can be used for a longer duration without frequent regeneration of the membrane. Our results suggest that the zeolite membranes (MCM-41, MCM-48 and FAU) are promising candidates for the separation of trivalent metal ions from aqueous solution based on interaction phenomena between the charged membrane and trivalent metal ions.

ACKNOWLEDGEMENTS

We would like to express our sincere gratitude to the Central Instruments Facility of IIT Guwahati for helping us to

perform FESEM analysis. The contact angle instrument used in this work was financially supported by a grant for the Center of Excellence for Sustainable Polymers at IIT Guwahati from the Department of Chemicals & Petrochemicals, Ministry of Chemicals and Fertilizers, Government of India.

REFERENCES

Ahmad, J. & Hagg, M. B. 2013 Preparation and characterization of polyvinyl acetate/zeolite 4A mixed matrix membrane for gas separation. *J. Membrane Sci.* **427**, 73–84.

Al-Rashdi, B. A. M., Johnson, D. J. & Hilal, N. 2013 Removal of heavy metal ions by nanofiltration. *Desalination* **315**, 2–17.

Arunkumar, A. & Etzel, M. R. 2015 Negatively charged tangential flow ultrafiltration membranes for whey protein concentration. *J. Membrane Sci.* **475**, 340–348.

Basumatary, A. K., Kumar, R. V., Ghoshal, A. K. & Pugazhenthi, G. 2015 Synthesis and characterization of MCM-41-ceramic composite membrane for the separation of chromic acid from aqueous solution. *J. Membrane Sci.* **475**, 521–532.

Danis, U. & Keskinler, B. 2009 Chromate removal from wastewater using micellar enhanced crossflow filtration: effect of transmembrane pressure and crossflow velocity. *Desalination* **249**, 1356–1364.

Frares, N. B., Taha, S. & Dorange, G. 2005 Influence of the operating conditions on the elimination of zinc ions by nanofiltration. *Desalination* **185**, 245–253.

Gherasim, C. V., Cuhorka, J. & Mikulasek, P. 2013 Analysis of lead (II) retention from single salt and binary aqueous solutions by a polyamide nanofiltration membrane: experimental results and modeling. *J. Membrane Sci.* **436**, 132–144.

Haarberg, G. M. & Keppert, M. 2008 Diffusion kinetics for the electrochemical reduction of Fe (III) species in molten NaCl-FeCl3. Presented at 214th Electrochemical Society Meeting, Abstract #3000.

Huang, A., Wang, N. & Caro, J. 2012 Seeding-free synthesis of dense zeolite FAU membranes on 3-aminopropltriethoxysilane-fucntionalized alumina supports. *J. Membrane Sci.* **389**, 272–279.

Iglesia, O. D. L., Pedernera, M., Mallada, R., Lin, Z., Rocha, J., Coronas, J. & Santamaria, J. 2006 Synthesis and characterization of MCM-48 tubular membranes. *J. Membrane Sci.* **280**, 867–875.

Jafarian, M., Mahjani, M. G., Gobal, F. & Danaee, I. 2006 Electrodeposition of aluminum from molten $AlCl_3$-NaCl-KCl mixture. *J. Appl. Electrochem.* **36**, 1169–1173.

Kumar, R. V., Basumatary, A. K., Ghoshal, A. K. & Pugazhenthi, G. 2015a Performance assessment of an analcime-C zeolite-ceramic composite membrane by removal of Cr (VI) from aqueous solution. *RSC Advances* **5**, 6246–6254.

Kumar, R. V., Moorthy, I. G. & Pugazhenthi, G. 2015b Modelling and optimization of critical parameters by hybrid RSM-GA for the separation of BSA using tubular configured MFI-type zeolite microfiltration membrane. *RSC Advances* **5**, 87645–87659.

Liu, C., Wang, L., Ren, W., Rong, Z., Wang, X. & Wang, J. 2007 Synthesis and characterization of a mesoporous silica (MCM-48) membrane on a large-pore α-Al_2O_3 ceramic tube. *Micropor. Mesopor. Mater.* **106**, 35–39.

Maghsoudi, H. & Soltanieh, M. 2014 Simultaneous separation of H_2S and CO_2 from CH_4 by a high silica CHA-type zeolite membrane. *J. Membrane Sci.* **470**, 159–165.

Majhi, A., Monash, P. & Pugazhenthi, G. 2009 Fabrication and characterization of α-Al_2O_3-clay composite ultrafiltration membrane for the separation of electrolytes from its aqueous solution. *J. Membrane Sci.* **340**, 181–191.

Mohammad, A. W., Othaman, R. & Hilal, N. 2004 Potential use of nanofiltration membranes in treatment of industrial wastewater from Ni-P electroless plating. *Desalination* **168**, 241–252.

Monash, P. & Pugazhenthi, G. 2011 Effect of TiO_2 addition on the fabrication of ceramic membrane supports: a study on the separation of oil droplets and bovine serum albumin (BSA) from its solution. *Desalination* **279**, 104–114.

Monash, P., Majhi, A. & Pugazhenthi, G. 2010 Separation of bovine serum albumin (BSA) using γ-Al_2O_3–clay composite ultrafiltration membrane. *J. Chem. Technol. Biotechnol.* **85**, 545–554.

Ozin, G. A., Kuperman, A. & Stein, A. 1989 Advanced zeolite materials science. *Adv. Mater.* **1**, 69–86.

Peeters, J. M. M., Boom, J. P., Mulder, M. H. V. & Strathmann, H. 1998 Retention measurements of nanofiltration membranes with electrolyte solutions. *J. Membrane Sci.* **145**, 199–209.

Sandstrom, L., Sjoberg, E. & Hedlund, J. 2011 Very high flux MFI membrane for CO_2 separation. *J. Membrane Sci.* **380**, 232–240.

Schaep, J., Bruggen, B. V. D., Vandecasteele, C. & Wilms, D. 1998 Influence of ion size and charge in nanofiltration. *Sep. Purif. Technol.* **14**, 155–162.

Shukla, A. & Kumar, A. 2007 Separation of Cr(VI) by zeolite-clay composite membranes modified by reaction with NOx. *Sep. Purif. Technol.* **52**, 423–429.

Wirawan, S. K., Creaser, D., Lindmark, J., Hedlund, J., Bendiyasa, I. M. & Sediawan, W. B. 2011 H_2 /CO_2 permeation through a silicalite-1 composite membrane. *J. Membrane Sci.* **375**, 313–322.

Workneh, S. & Shukla, A. 2008 Synthesis of sodalite octahydrate zeolite-clay composite membrane and its use in separation of SDS. *J. Membrane Sci.* **309**, 189–195.

Wu, S., Yang, J., Lu, J., Zhou, Z., Kong, C. & Wang, W. 2008 Synthesis of thin and compact mesoporous MCM-48 membrane on vacuum-coated α-Al_2O_3 tube. *J. Membrane Sci.* **319**, 231–237.

Yu, M., Falconer, J. L., Amundsen, T. J., Hong, M. & Noble, R. D. 2007 A controllable nanometer sized valve. *Adv. Mater.* **19**, 3032–3036.

First received 12 December 2015; accepted in revised form 28 January 2016. Available online 17 March 2016